Turkish Journal of Electrical Engineering & Computer Sciences

http://journals.tubitak.gov.tr/elektrik/

Research Article

Turk J Elec Eng & Comp Sci
(2017) 25: 2647 – 2659

doi:10.3906/elk-1606-63

Time-time matrix z-score vector-based fault analysis method for series-compensated transmission lines

Oveis ASGARI GASHTEROODKHANI, Behrooz VAHIDI*, Aydin ZABOLI
Department of Electrical Engineering, Amirkabir University of Technology, Tehran, Iran

Received: 05.06.2016 • **Accepted/Published Online:** 02.10.2016 • **Final Version:** 30.07.2017

Abstract: In this paper, a novel protection method based on time-time (TT) transform for thyristor-controlled series-compensated lines is presented. First, current signals at both sides of the sending and receiving ends are retrieved and processed through time-time domain transform (TT-transform), and a TT-matrix is produced. A proposed index is then compared with a defined threshold (THD) in order to determine fault occurrence and faulted phases. Within less than three cycles of the fault inception, a tripping signal can be sent that is acceptable for the speed of digital relays. After faulted phase selection, considering the TT-matrix of the faulted phases of both the sending and receiving ends, another index is introduced for estimation of the fault section. Simulation results show that this approach determines fault occurrence, faulted phase, and fault section under different fault conditions such as fault type, fault location, fault resistance, fault inception angle, source impedance, reverse power flow, different levels of compensation, and different locations of the compensator in the line. The test results in the presence of high noise (with SNR up to 15 dB) confirm the effectiveness of the proposed method. The results also indicate that the proposed method is more robust to fault resistance compared to previous studies.

Key words: Thyristor-controlled series compensator, TT-transform, transmission line protection, fault occurrence, faulted phase selection, fault section estimation

1. Introduction

In recent years, because of environmental and energy-related issues, transmission line installation and new power productions are hindered. Therefore, increasing the capability of conventional transmission lines instead of new line installation is essential. As a result, power flow control in transmission lines is very important for covering power transmission requirements [1]. The thyristor-controlled series compensator (TCSC) is one of the most important FACTS devices that has the capability to develop conventional transmission systems. TCSC-based compensation includes variable capacitors that are controlled by thyristors and protected by a metal oxide varistor (MOV) and an air gap. However, using a TCSC can affect the line apparent impedance [2–4] that is controlled by the thyristor triggering angle, and this phenomenon can be intensified by factors like the MOV. Additionally, the presence of a TCSC in a fault loop affects both the constant components and the transient ones. The MOV, controllable reactance, and air-gap actions make the protection decision more complicated. Therefore, it creates some problems in protection planning based on relay fixed settings [5]. Fault classification and determination of fault sections in a transmission line with the presence of FACTS devices are challenging.

*Correspondence: vahidi@aut.ac.ir

Many attempts have been made at fault classification and fault section estimation using wavelet transform, Kalman filters, and neural networks [6–12].

In the Kalman approach, [9] fault resistance cannot be modeled, and the use of various filters is also essential. Neural network-based fault classification approaches [11,12] need a wide range of training, too much training time, and the design of a neural network for each transmission system. The wavelet transform [6–8] has been introduced as a useful method for transmission line protection with the use of time and frequency domain analysis. In [13], the Morlet wavelet was used to determine high impedance faults and differentiate them from switching events. In [14,15] a combination of wavelet transform and the support vector machine (SVM) was used for fault section identification in a TCSC-based transmission line. The wavelet packet transform was used to provide protection for a TCSC-based compensated line [9]. In those works, the wavelet transform was very sensitive to noise and the results were not exact, even with SNR up to 30 dB [10]. The authors of [11] proposed a protection scheme for parallel transmission lines using the S-transform, which is more immune to noise; however, it does not consider compensated transmission lines. In [5] a protection method for a transmission line with a TCSC was presented with the use of a differential energy-based (S-transform) method based on a set threshold so as to send tripping signals. However, in [5], there should be different set thresholds for different fault conditions, and since the presented index in [5] (differential energy) was not calculated on a per unit system, the method is required to select different thresholds for networks with different configurations.

Recently, the TT-transform derived from the S-transform was presented in signal processing [16]. The TT-transform decomposes 1D time series to 2D time-time series. In recent years, the TT-transform has been used in power systems for fault detection [17], power quality events [18], and transformer protection [19]. The TT-transform has a great ability to amplify high-frequency components of fault currents. Thus, it is known as a strong tool for detecting faults in power systems [20]. This paper presents a new method for fault detection, classification, and section estimation in a transmission line including a TCSC using TT-transform. The proposed method consists of two parts. In the first part, fault currents are calculated in both ends of the transmission line. Then, with the use of the TT-transform for current signals of both the sending and receiving ends, the TT-matrix for each phase is obtained. An index based on a TT-matrix z-score vector is then considered and, by comparing it with a threshold (THD), the fault occurrence and faulted phase can be determined. Therefore, in this step, the tripping signal can be sent to a digital relay within three cycles just after the fault occurrence based on a determined THD. In the next step, after fault detection, by considering the TT-matrix for each phase, another index is used to determine the fault section. In the assumed transmission line including the TCSC, the TCSC is placed exactly in the middle of the line. Thus, with this assumption, our meaning of fault section estimation is whether a fault occurs before the TCSC or after it (from the view of the relay, which is on the sender side). In other words, it determines whether the fault loop encompasses the TCSC or not and therefore the fault section is determined in relation to the TCSC. In this paper, it is assumed that the obtained currents from the two terminals are synchronized in time. This synchronous measurement is performed using a GPS system with very high accuracy (1 μs).

The proposed method gives us highly acceptable results under different operating conditions. Moreover, the effectiveness of the proposed method in high-noise conditions is checked. The results show the promising performance of the proposed method in the presence of high noise and high fault resistance, which is an advantage of the proposed method compared to previous methods. In the rest of the paper, the TT-transform, the considered system, the simulation results, and the discussion and conclusion are described.

2. TT-transform

The TT-transform is a two-dimensional time-time representation of a one-dimensional time series. To have a better understanding of the TT-transform theory, we start with the short-time Fourier transform (STFT). The STFT is expressed by the following equation [16,18]:

$$STFT\left(t,f\right)=\int_{-\infty}^{\infty}h\left(\tau\right)w\left(t-\tau\right)e^{-2\pi if\tau}d\tau, \tag{1}$$

where $h(\tau)$ is the signal that should be transformed and $w(\tau)$ is the window function whose position is determined by t. τ and f represent time and frequency, respectively. Another form of Eq. (1) is obtained using the convolution theorem as below:

$$STFT(t,f)=\int_{-\infty}^{+\infty}H(\alpha+f)\,W(\alpha)e^{2\pi i\alpha t}d\alpha, \tag{2}$$

where W and α denote the Fourier transform of w and the convolution variable, respectively. α has the same unit as f.

The STFT has some disadvantages, such as the fixed width and height of the window. By replacing the window function $w(\tau)$ of the STFT with the Gaussian function given in Eq. (3), the S-transform is derived from Eq. (1) as follows:

$$\omega(\tau)=\frac{|f|}{\sqrt{2\pi}}\exp(\frac{-f^2\tau^2}{2}), \tag{3}$$

$$S\left(t,f\right)=\int_{-\infty}^{\infty}h\left(\tau\right)\frac{|f|}{\sqrt{2\pi}}e^{\left(\frac{-f^2(t-\tau)^2}{2}\right)}e^{-2\pi if\tau}d\tau. \tag{4}$$

An alternative form of the S-transform can be written the same as in Eq. (2):

$$S\left(t,f\right)=\int_{-\infty}^{\infty}H\left(\alpha+f\right)e^{\left(\frac{-2\pi^2\alpha^2}{f^2}\right)}e^{2\pi i\alpha t}d\alpha. \tag{5}$$

The TT-transform is defined as the inverse Fourier transform of the S-transform as follows:

$$TT\left(t,\tau\right)=\int_{-\infty}^{\infty}S\left(t,f\right)e^{+2\pi if\tau}df. \tag{6}$$

If $h[kT],k=0,1,\ldots,N-1$ is the discrete form of the signal $h(\tau)$ with sampling interval of T, the discrete Fourier transform of $h[kT]$ is obtained as follows:

$$H\left[\frac{m}{NT}\right]=\frac{1}{N}\sum_{k=0}^{N-1}h[kT]\,e^{-\frac{i2\pi mk}{N}}, \tag{7}$$

where $m = 0, 1, 2, \ldots, N$, and N is the number of samples of the signal. By replacing f with n/NT and t with jT in Eq. (4), the discrete S-transform of $h[kT]$ is given as follows:

$$S\left[jT, \frac{n}{NT}\right] = \sum_{m=-N/2}^{N/2-1} H\left[\frac{m+n}{NT}\right] e^{\left[\frac{-2\pi^2 m^2}{n^2}\right]} e^{\left[\frac{2\pi imj}{NT}\right]}, \quad j, m, n = 0, 1, 2, ..., N-1. \tag{8}$$

Thus, the discrete TT-transform can be written as follows:

$$TT\left[jT, kT\right] = \sum_{m=-N/2}^{N/2-1} S\left[jT, \frac{n}{NT}\right] e^{\left[\frac{2\pi ink}{N}\right]}. \tag{9}$$

3. Case study

In this paper, a power transmission system has been simulated using the MATLAB/Simulink software package. The power system includes a TCSC as shown in Figure 1 [5,9]. The value of sampling frequency is 1 kHz at base frequency of 50 Hz so that one cycle of the faulted current signals contains 20 samples. The distributed parameter line model considering the circuit impedance and admittance to be distributed over the entire circuit is used in this study. The TCSC located at the midpoint of the transmission line is designed to supply different levels of compensation. The data of the power transmission system are given in Table 1.

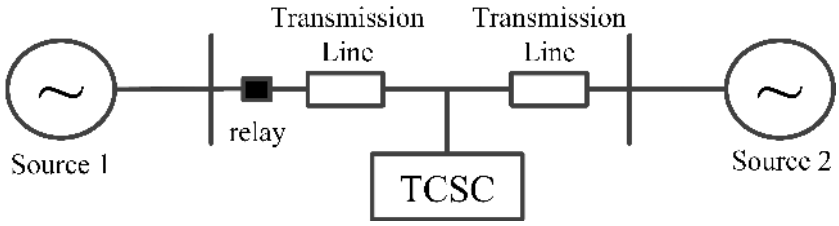

Figure 1. Power system.

Table 1. Power system data.

Parameters	Values
Length of transmission line	300 km
Base frequency	50 Hz
Rated voltage	400 kV
Zero sequence impedance	96.45 + j335.26 Ω
Positive sequence impedance	9.78+ j110.23 Ω
Zero sequence capacitance	2.32 μF
Positive sequence capacitance	3.82 μF
Source-1 voltage	$400\angle\delta_1$ kV, $\delta_1 = 60^\circ$
Source-2 voltage	$400\angle\delta_2$ kV, $\delta_2 = 0$
Sampling frequency	1 kHz

Figure 2 shows the basic circuit of a TCSC. In this circuit, the goal of the MOV is to prevent the capacitor voltage from reaching a dangerous level. When the capacitor voltage reaches a hazardous level,

the MOV conducts a significant portion of the fault current. If the energy and temperature of the MOV in conduction mode meet the emergency mode, an air gap is designed to bypass the MOV and the capacitor.

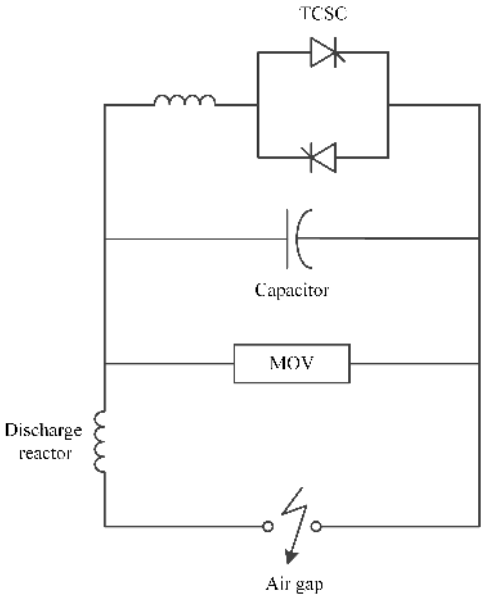

Figure 2. TCSC model.

4. Simulation results

4.1. Feature extraction

Due to the presence of harmonics in fault current signals including the TCSC, the decision-making process during a fault is affected [5]. In the proposed method, fault current signals are measured in both the sender and receiver sides of the transmission line, and using the TT-transform, a time-time contour is obtained. Produced contours and fault currents for different faults are shown in Figures 3 and 4, respectively. From Figure 3, it is obvious that the produced contours show the fault exactly after the occurrence. It is also observed that the currents from the sender (Figure 4a) and receiver (Figure 4b) sides for the same fault (a-b-c-g, at 30% of the line before the TCSC with fault resistance of $R_f = 20\ \Omega$, and fault inception angle of $\alpha = 45^\circ$) are very different from each other. The reason for this is that the receiver side sees the fault current including the TCSC. Thus, some harmonics are inside the fault current at the receiver side while the sender side does not see the fault current including the TCSC. Similar results are observed for the sender (Figure 4c) and the receiver (Figure 4d) sides for another fault (a-b-g, at 75% of the line after TCSC with $R_f = 30\ \Omega$ and $\alpha = 30^\circ$). In contrast with the last one, this time, the sender side sees the fault current including the TCSC, and the receiver side sees the fault current not including the TCSC.

4.2. Fault detection and faulted phase selection

First, using the TT-transform for currents of both the sender and receiver sides of the transmission line, the TT-matrix ($M \times N$) for each phase can be computed. After that, the z-score of the TT-matrix is calculated. The z-score is defined as a statistical measurement from the correlation of a group of information and the mean of that group [20]. An index based on the z-score is then introduced for fault detection and faulted phase selection. For determination of the z-score of the TT-matrix, initially, the absolute value of the TT-matrix ($|TT[k, L]|$)

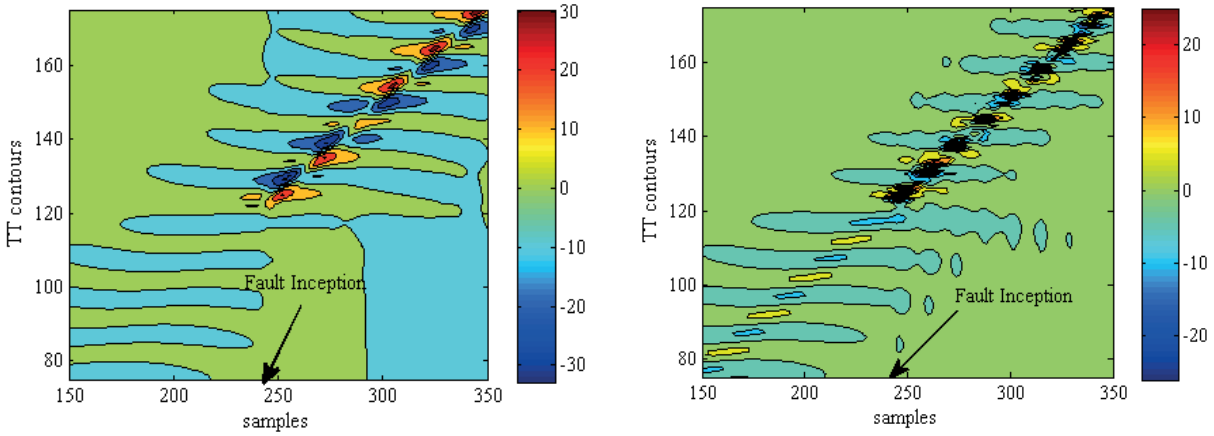

Figure 3. TT-contour of phase a at sending end (a) for a-b-c-g fault at 30% of line, $R_f = 20\ \Omega$, $\alpha = 105^\circ$; (b) for a-b-c-g fault at 70% of line, $R_f = 25\ \Omega$, $\alpha = 95^\circ$.

is calculated. Then, having considered the columns of $|TT[k,L]|$, the mean and the standard deviation (STD) values of them are calculated as given in Eqs. (10) and (11), respectively.

$$TTM\left[1,L\right] = \sum_{k=1}^{M} \frac{\left|TT\left[k,L\right]\right|}{M} \quad , \quad L = 1,...,N \tag{10}$$

$$TTst\left[1,L\right] = \left\{ \frac{1}{M-1} \sum_{k=1}^{M} \left|TT\left[k,L\right]\right| - TTM\left[1,L\right] \right\}^{1/2} \quad , \quad L = 1,...,N \tag{11}$$

Here, TTM and $TTst$ represent the vectors including the mean and the STD of each column of $|TT[k,L]|$, respectively. The TT-transform z-score matrix is written as follows:

$$TTzs\left[k,L\right] = \left| \left\{ \frac{\left|TT\left[k,L\right]\right| - TTM\left[1,L\right]}{TTst\left[1,L\right]} \right\} \right| \quad , \quad k = 1,...,M, \quad L = 1,...,N, \tag{12}$$

where $TTzs$ is an $M \times N$ matrix indicating the TT-transform z-score matrix. The z-score vector of the TT-matrix ($TTzv$) is a vector with length of N as given below:

$$TTzv\left[1,L\right] = \sum_{k=1}^{M} TTzs\left[k,L\right] \ , \ L = 1,...,N. \tag{13}$$

After calculation of $TTzv$ for each three phases of both the sender and receiver sides of the transmission line, the phase selection index (PSI) is calculated as follows:

$$PSI_i = \frac{TTzv_{RS-i}}{\max\left(\max\left(TTzv_{RS-a}\right), \max\left(TTzv_{RS-b}\right), \max\left(TTzv_{RS-c}\right)\right)} \quad , \quad for\ i = a,\ b,\ c, \tag{14}$$

where $TTzv_{RS-i}$ is obtained by the following formula:

$$TTzv_{RS-i} = \left|TTzv_{S-i} - TTzv_{R-i}\right| \quad , \quad for\ i = a,b,c, \tag{15}$$

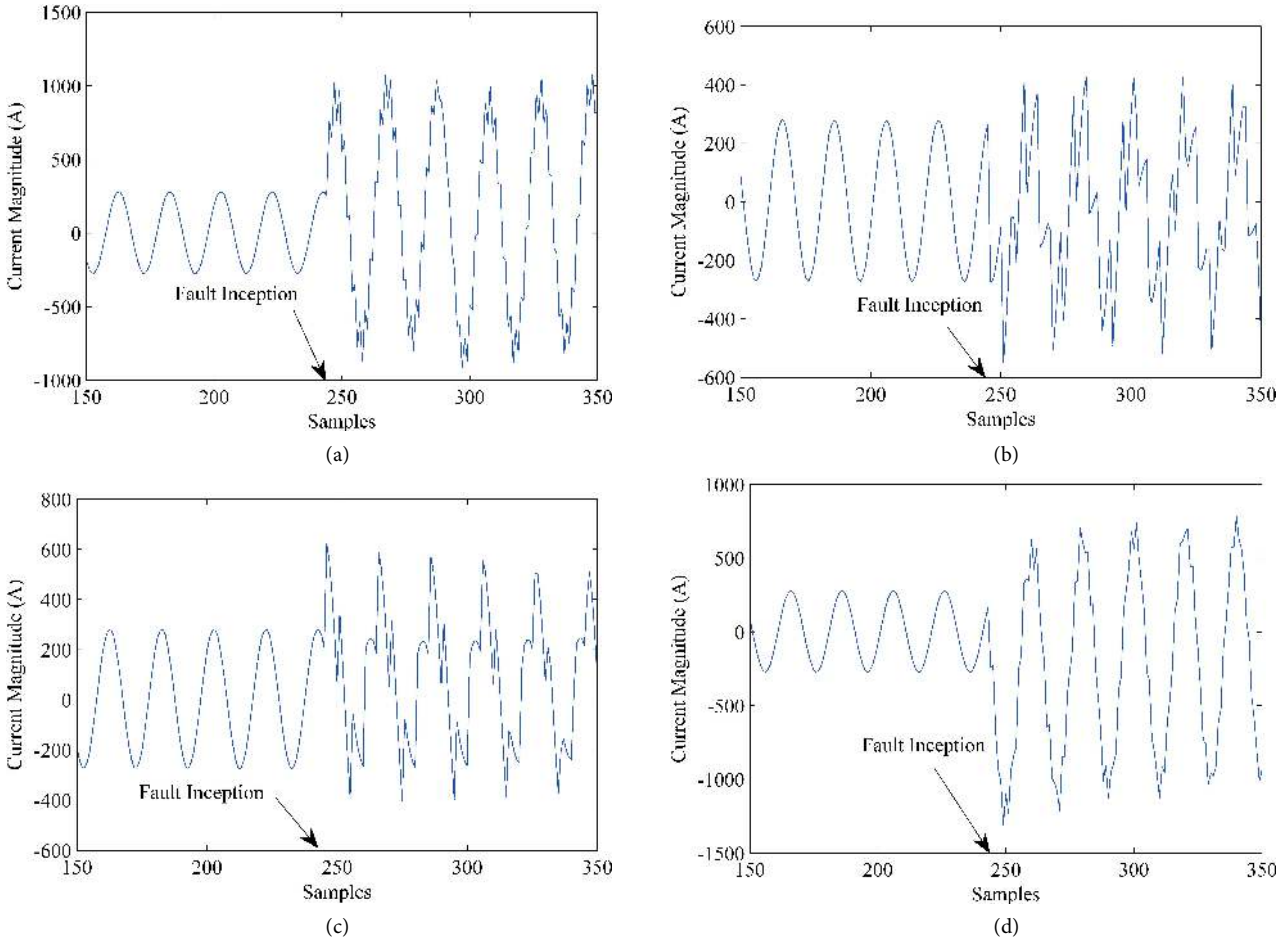

Figure 4. Fault current of phase a (a) at sending end for a-b-c-g fault at 30% of line, Rf =20 Ω, $\alpha = 45^\circ$; (b) at receiving end for a-b-c-g fault at 30% of line, Rf =20 Ω, $\alpha = 45^\circ$; (c) at sending end for a-b-g fault at 75% of line, Rf =30 Ω, $\alpha = 30^\circ$; (d) at receiving end for a-b-g fault at 75% of line, Rf =30 Ω, $\alpha = 30^\circ$.

where $TTzv_{R-i}$ and $TTzv_{S-i}$ are TT-matrix z-score vectors of the receiver and sender sides for phase-i (i = a, b, c), respectively.

4.3. Effects of different fault conditions

Fault types, fault resistance, fault inception angle, fault position, source impedance, reverse power flow, and different levels of compensation highly affect fault processes in transmission lines. Figure 5 shows the PSI for different fault types. Figure 5a shows a single-phase fault (a-g, at 30% of the line before the TCSC and with $R_f = 50$ Ω and $\alpha = 120^\circ$). According to Figure 5a, because the fault is in phase a, the PSI vector for this phase increases in comparison with other phases. Figure 5b shows the PSI vector for a line-line-ground fault (a-b-g, at 70% of the line after the TCSC and with R_f =70 Ω and $\alpha = 90^\circ$). It is observed that the PSI vector for both phase a and phase b grows while the PSI vector for the other phase (phase c) stays near zero. Figure 5c shows the PSI index for a line-line-line-ground fault (a-b-c-g, at 80% of the line after the TCSC and with R_f =20 Ω and $\alpha = 100^\circ$). In this one, the index is increasing for each of the three phases. Consequently, it shows that all phases are involved in the fault process.

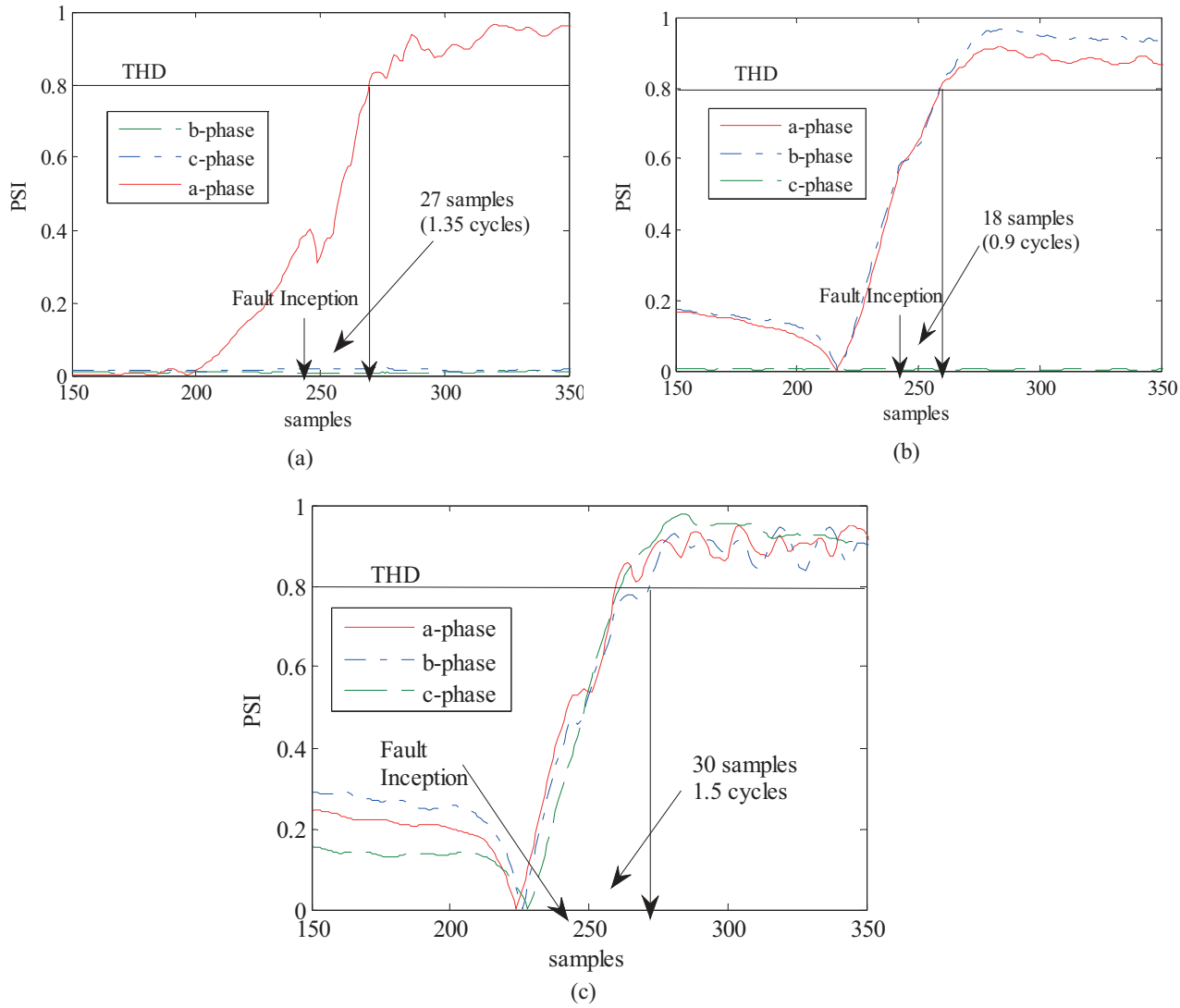

Figure 5. PSI for different fault types: (a) PSI for a-g fault at 30% of line before TCSC, R_f =50 Ω, α = 125°; (b) PSI for a-b-g fault at 70% of line after TCSC, R_f =70 Ω, α = 95°; (c) PSI for a-b-c-g fault at 80% of line after TCSC, Rf =20 Ω, α = 105°.

Fault resistance has considerable effects on the fault process. Figure 6 shows the PSI vector of phase a for a line-ground fault (a-g, at 30% of the line with α = 20°) with different fault resistances (R_f =10, 50, 100, 200 Ω) for the proposed method and the differential energy-based method [5]. Noting Figure 6, it can be observed that the proposed method for different fault resistances has an acceptable performance while the differential energy-based method fails in detecting faults with higher fault resistance. This is due to the fact that the proposed method uses a normalized index (PSI) that is more robust to changes in fault resistance while the value of differential energy index is considerably reduced for higher fault resistances.

The effects of some other fault conditions on the proposed index are shown in Figure 7. Figure 7a shows the PSI vector of phase a for a line-line-ground fault (a-b-g, at 90% of the line after the TCSC, with R_f =70 Ω and α = 90°) for three states of normal, 30% increment, and 30% decrement in source impedance. Noting

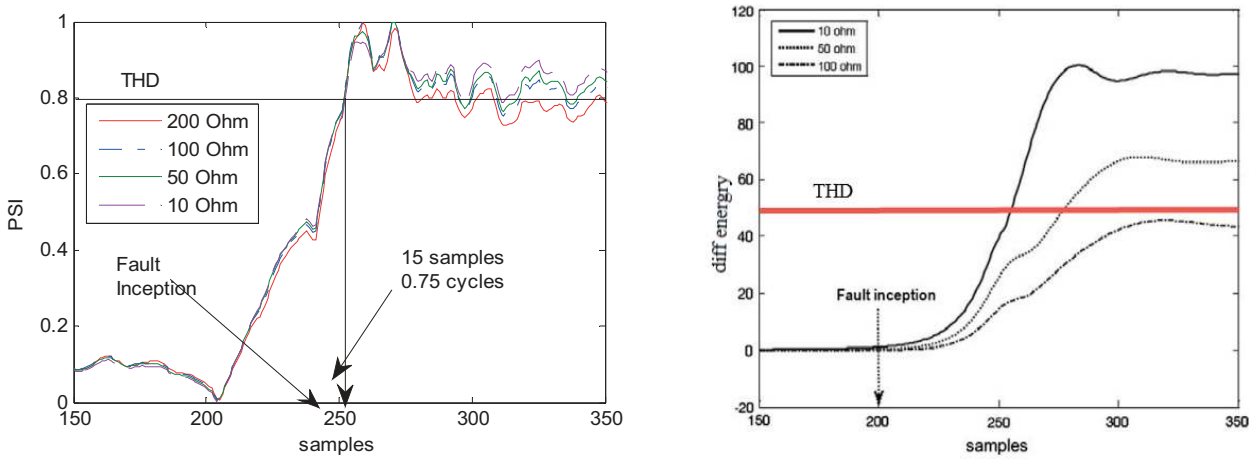

Figure 6. Effects of fault resistance: (a) proposed method, (b) differential energy-based method [5].

Figure 7a, it can be observed that source impedance tolerance does not affect the performance of the proposed method. Figure 7b shows the PSI vector of phase a for a line-ground fault (a-g, at 30% of the line before the TCSC and with $R_f = 100\ \Omega$ and $\alpha = 80°$) with 25%, 50%, and 75% compensation levels. Noting Figure 7b, it is observed that THD can be determined to issue tripping signals for different levels of compensation. Figure 7c shows the effect of reverse power flow on a line-ground fault (b-g, at 55% of the line after the TCSC, and with $R_f = 50\ \Omega$ and $\alpha = 30°$). Noting Figure 7c, it is observed that when the line has reverse power flow, by selecting a proper THD, a tripping signal can be sent. Figure 7d shows phase a for a three-phase fault (a-b-c-g at 70% of the line with $R_f = 25\ \Omega$ and $\alpha = 90°$) with different positions of the TCSC in 25%, 50%, and 90% of the transmission line. According to Figure 7d, the position of the TCSC in the transmission line does not influence the performance of the presented method. After simulation of various fault conditions, a threshold setting of 0.8 is selected for the transmission line including the TCSC. By considering the above observations, it can be concluded that different types of fault under various operating conditions are determinable within two cycles from fault inception by the proposed index based on the mentioned threshold. Moreover, since the PSI is a normalized index, the chosen threshold is suitable for other operating conditions of the network.

4.4. Fault section estimation

Here the purpose of fault section estimation is to determine the fault position in association with the TCSC, i.e. whether the fault occurs before or after the TCSC. In other words, we want to know whether the fault loop contains the TCSC or not. For this purpose, after determination of faulted phases, the results of applying the TT-transform to each of the faulted phases of the sender and the receiver sides are considered, and the $TTzv$ value for each phase is obtained. Then, according to the following equation, by adding all elements of $TTzv$, TTz is obtained:

$$TTz = \sum_{L=1}^{N} TTzv\,[1, L]. \tag{16}$$

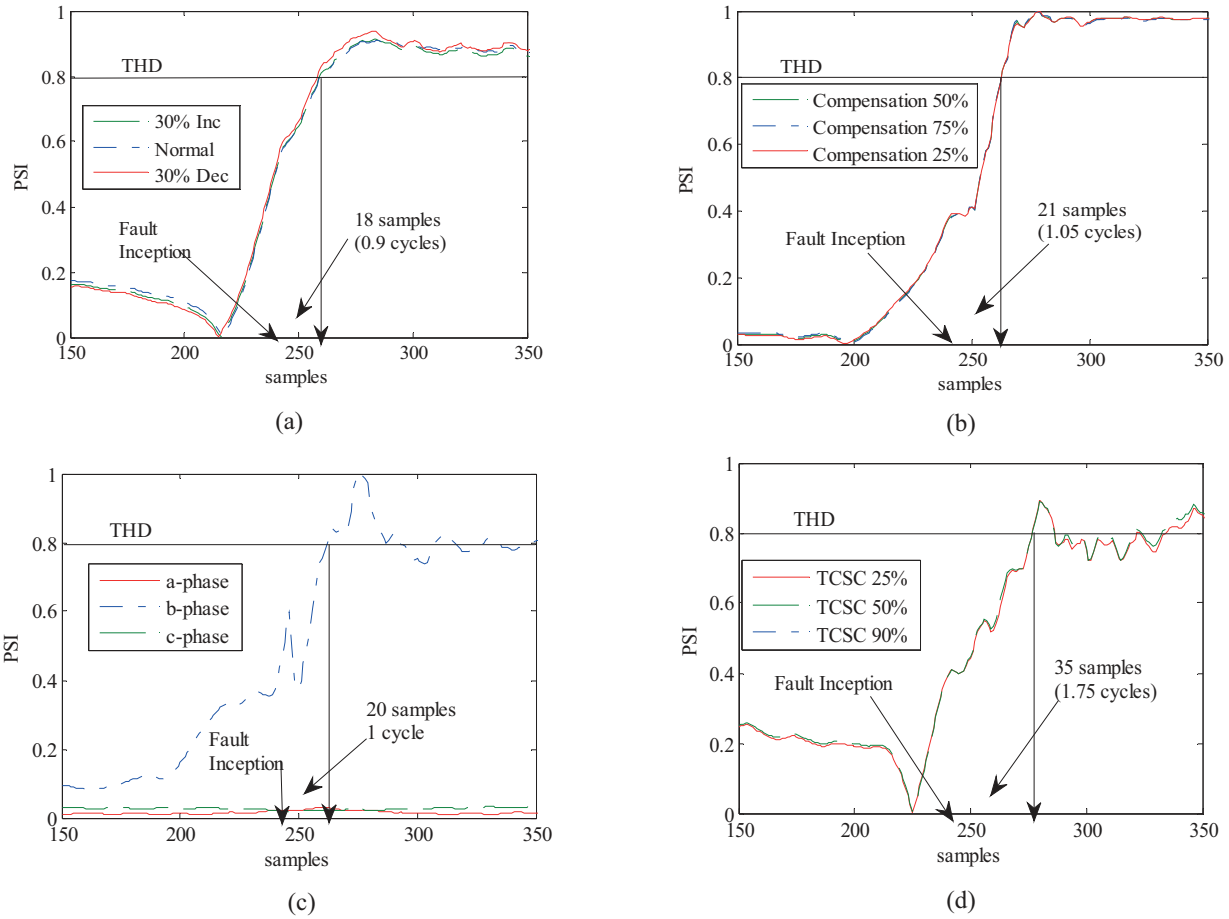

Figure 7. Effects of different fault conditions: (a) PSI for a-b-g fault at 90% of line, Rf =70 Ω, $\alpha = 90^\circ$ with three states of normal, 30% increment, and 30% decrement in source impedance; (b) PSI for a-g fault at 30% of line before TCSC, Rf =100 Ω, $\alpha = 80^\circ$ with 25%, 50%, and 75% compensation levels; (c) PSI for b-g fault at 55% of line, Rf =50 Ω, $\alpha = 30^\circ$ with reverse power flow ($\delta 1 = 0$, $\delta 2 = 60^\circ$); (d) PSI for a-b-c-g at 70% of line, Rf =25 Ω, $\alpha = 90^\circ$ with different positions of TCSC in 25%, 50%, and 90% of line.

Now the difference of TTz_S at the sender side and TTz_R at the receiver side is introduced as the fault section identification index (SII):

$$SII = TTz_S - TTz_R \tag{17}$$

Now, if the index is a positive value, it means that the fault occurred before the TCSC, and if it is negative, it means that the fault occurred after the TCSC. This is because the values of the TT-matrix and as a result TTz are higher for the end that is closer to the fault location. Table 2 shows the determination of the fault section using the proposed index for different operating conditions. With respect to Table 2, it is observed that in all cases, the fault section is correctly predicted using the proposed method.

4.5. Checking the effects of noise

According to [10,20], wavelet transform-based methods such as those from [6–8] could be affected by noise even with SNR up to 30 dB. In this paper, in order to evaluate the performance of the proposed protection method in a noisy environment, the TT-transform is applied to the current signals contaminated by noise with SNR of

Table 2. SII for different fault conditions.

Fault type	Fault location	Fault resistance (Ω)	Fault inception angle (degrees)	Compensation level	Power state	SII
a-g	30%	30	30	50%	Normal	Positive
a-g	30%	50	60	75%	Reverse	Positive
a-g	75%	100	30	50%	Reverse	Negative
a-b-g	25%	30	30	50%	Normal	Positive
a-b-g	25%	50	60	75%	Reverse	Positive
a-b-g	80%	70	45	25%	Normal	Negative
a-b-g	80%	100	30	50%	Reverse	Negative
a-b-c-g	20%	30	30	50%	Normal	Positive
a-b-c-g	20%	50	60	75%	Reverse	Positive

15 dB. Figure 8 shows an a-b-c-g fault at 80% transmission line after the TCSC with R_f =20 Ω and $\alpha = 40^\circ$ in high noise with SNR = 15 dB. According to Figure 8, the tripping signal can be sent within 2.5 cycles after fault inception. Thus, the results validate the superiority of the proposed method over wavelet-based methods in noisy conditions.

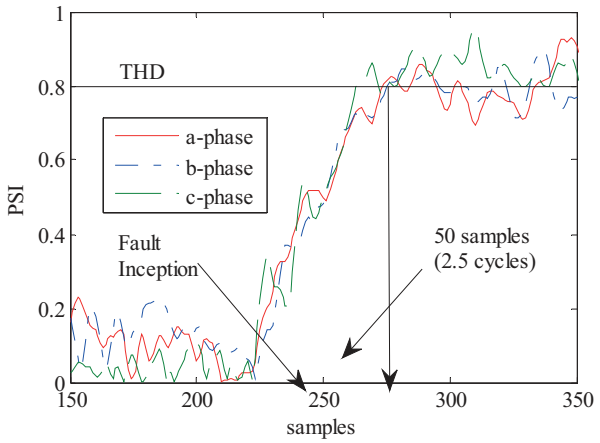

Figure 8. PSI for a-b-c-g, at 80% of line after TCSC, with R_f =20 Ω, $\alpha = 40^\circ$, SNR = 15 dB.

5. Discussion

For fault detection and faulted phase determination by simulating various fault conditions before and after the TCSC in a transmission system including the TCSC, the threshold value is selected as 0.8 (THD = 0.8), which is suitable for different fault conditions. By selecting the mentioned threshold, a tripping signal can be sent within three cycles after fault inception. Therefore, the proposed method provides the required speed for protective relays. However, in order to have higher reliability, a larger threshold value can be chosen, but it leads to a delay in sending the trip. In the existing work [5], different thresholds were selected for protection of a TCSC-based transmission line against the faults including the TCSC and the faults not including the TCSC. However, the proposed protection method sets a unique threshold, which is independent of the fault position. This is owing to the fact that, unlike in [5], the suggested index (PSI_i) is calculated on a per unit system. This clearly indicates that the presented method is more suitable for the decision-making process. More importantly, since the PSI is calculated on a per unit scale, the selected THD is suitable for TCSC-based lines with different

configurations. The impact of high noise on the presented approach performance has also been investigated. The results confirm that the proposed method has better performance compared to wavelet transform-based methods in a noisy environment.

6. Conclusion

In this paper, a protection method based on the TT-transform in a compensated transmission line including a series FACTS device (TCSC) is proposed. An index based on the z-score of a TT-matrix for fault detection and faulted phase selection is introduced so that determining an appropriate threshold (THD) can send the tripping signal within three cycles from fault occurrence. Another index is also introduced for fault section estimation in association with the TCSC. The proposed method is tested on various fault conditions (including different types of faults, fault location, fault resistance, fault inception angle, source impedance, various levels of compensation, and different positions of the TCSC in the transmission line and effects of reverse power flow). In all the cases mentioned, the simulation results show the suitable performance of the proposed method.

References

[1] El-Zonkoly AM, Desouki H. Wavelet entropy based algorithm for fault detection and classification in FACTS compensated transmission line. Int J Elec Power 2011; 33: 1368-1374.

[2] Zhou X, Wang H, Aggarwal R, Beaumont P. Performance evaluation of a distance relay as applied to a transmission system with UPFC. IEEE T Power Deliver 2006; 21: 1137-1147.

[3] Khederzadeh M, Sidhu TS. Impact of TCSC on the protection of transmission lines, IEEE T Power Deliver 2006; 21: 80-87.

[4] Sadeh J, Adinehzadeh A. Accurate fault location algorithm for transmission line in the presence of series connected FACTS devices. Int J Elec Power 2010; 32: 323-328.

[5] Samantaray S, Tripathy L, Dash P. Differential energy based relaying for thyristor controlled series compensated line. Int J Elec Power 2012; 43: 621-629.

[6] Shaik AG, Pulipaka RRV. A new wavelet based fault detection, classification and location in transmission lines. Int J Elec Power 2015; 64: 35-40.

[7] Yadav A, Swetapadma A. A single ended directional fault section identifier and fault locator for double circuit transmission lines using combined wavelet and ANN approach. Int J Elec Power 2015; 69: 27-33.

[8] Mahari A, Seyedi H. High impedance fault protection in transmission lines using a WPT-based algorithm. Int J Elec Power 2015; 67: 537-545.

[9] Samantaray S, Dash P. Wavelet packet-based digital relaying for advanced series compensated line. IET Gener Transm Dis 2007; 1: 784-792.

[10] Yang HT, Liao CC. A de-noising scheme for enhancing wavelet-based power quality monitoring system. IEEE T Power Deliver 2001; 16: 353-360.

[11] Dash P, Samantaray S, Panda G, Panigrahi B. Time–frequency transform approach for protection of parallel transmission lines. IET Gener Transm Dis 2007; 1: 30-38.

[12] Mathur RM, Varma RK. Thyristor-Based FACTS Controllers for Electrical transmission Systems. New York, NY, USA: John Wiley & Sons, 2002.

[13] Huang SJ, Hsieh CT. High-impedance fault detection utilizing a Morlet wavelet transform approach. IEEE T Power Deliver 1999; 14: 1401-1410.

[14] Parikh UB, Das B, Maheshwari RP. Combined wavelet-SVM technique for fault zone detection in a series compensated transmission line. IEEE T Power Deliver 2008; 23: 1789-1794.

[15] Parikh UB, Das B, Maheshwari R. Fault classification technique for series compensated transmission line using support vector machine. Int J Elec Power 2010; 32: 629-636.

[16] Pinnegar CR, Mansinha L. A method of time–time analysis: the TT-transform. Digit Signal Process 2003; 13: 588-603.

[17] Samantaray S, Panigrahi B, Dash P. High impedance fault detection in power distribution networks using time–frequency transform and probabilistic neural network. IET Gener Transm Dis 2008; 2: 261-270.

[18] Suja S, Jerome J. Pattern recognition of power signal disturbances using S Transform and TT Transform. Int J Elec Power 2010; 32: 37-53.

[19] Ashrafian A, Vahidi B, Mirsalim M. Time–time-transform application to fault diagnosis of power transformers. IET Gener Transm Dis 2014; 8: 1156-1167.

[20] Ahmadimanesh A, Shahrtash S. Time-time-transform-based fault location algorithm for three-terminal transmission lines. IET Gener Transm Dis 2013; 7: 464-473.